Excitation function measurement for zirconium-89 and niobium-90 production using alpha-induced reactions on yttrium-89

T. Murata[a,*], M. Aikawa[a,b], M. Saito[a], H. Haba[c], Y. Komori[c], N. Ukon[d], S. Takács[e], F. Ditrói[e]

[a] *Graduate School of Biomedical Science and Engineering, Hokkaido University, Sapporo 060-8638, Japan*
[b] *Faculty of Science, Hokkaido University, Sapporo 060-0810, Japan*
[c] *Nishina Center for Accelerator-Based Science, RIKEN, Wako 351-0198, Japan*
[d] *Advanced Clinical Research Center, Fukushima Medical University, Fukushima City 960-1295, Japan*
[e] *Institute for Nuclear Research, Hungarian Academy of Sciences (ATOMKI), 4026 Debrecen, Hungary*

Abstract

An experiment of α-induced reactions on yttrium-89 was performed to investigate the excitation functions of ^{89}Zr and ^{90}Nb, which are suitable for immuno-PET studies. The stacked-foil method, activation technique, and off-line γ-ray spectrometry were used for this investigation. The excitation functions of ^{92m,91m,89m,89g}Nb, ^{88}Zr, and ^{90m,88g,87m,87g}Y were also derived and compared with earlier experimental and the TENDL-2017 data. Good agreements with part of the previous studies were found.

Keywords: Yttrium, Alpha particle, Excitation function, Immuno-PET, Zirconium-89, Niobium-90

1. Introduction

Recently, a novel technique called "immuno-PET" is attracting attentions as a powerful tool in companion diagnostics, individualized treatments, and efficient drug developments[1, 2, 3, 4]. As a radionuclide used for immuno-

*Corresponding author
Email address: murata@nds.sci.hokudai.ac.jp (T. Murata)

PET, ^{89}Zr is highly expected due to its suitable physical half-life, the emitted positrons' energy and the developing labeling technique to an antibody[4, 5, 6]. From the point of view of the radionuclide production, it is important to investigate what reaction is the most efficient and how much activities can be obtained by that reaction. There are several options to create ^{89}Zr such as ^{89}Y(p, n), ^{89}Y(d, 2n), ^{89}Y(α, x), and $^{\mathrm{nat}}$Sr(α, x) reactions. Although the ^{89}Y(p, n) reaction is promising for the ^{89}Zr production, it is worthwhile to investigate other reactions using heavier particles.

The ^{89}Y(α, x) reaction can simultaneously generate ^{89}Zr and ^{90}Nb. Niobium-90 is another expectable radionuclide for immuno-PET[7, 8]. To determine the yields of ^{89}Zr and ^{90}Nb produced by using this reaction, the excitation function data are quite basic and important. Three previous experiments were found for the ^{89}Y(α, x)^{89}Zr reaction[9, 10, 11], and five for the ^{89}Y(α, x)^{90}Nb reaction[9, 10, 11, 12, 13] in the EXFOR library[14]. However, there are discrepancies among the experimental data of these excitation functions. This situation causes high uncertainties in the evaluation of the yields. Therefore, we were motivated to investigate α-induced reactions on yttrium-89. The cross sections of the radionuclides other than ^{89}Zr and ^{90}Nb were also measured and reported in this paper. The results were compared with the earlier experimental data and the theoretical calculations. The data from the TENDL-2017 library[15], which is based on the TALYS code, were used as theoretical calculations for systematic comparison.

2. Material and methods

The well-known stacked-foil technique, activation method, and off-line γ-ray spectrometry were adopted to measure the excitation functions for α-induced reactions on yttrium-89. The experiment was performed at Nishina Center for Accelerator-Based Science, RIKEN, Wako.

2.1. Target preparation

Three kinds of metallic foils were prepared; yttrium-89 (25 μm; 99% purity; Goodfellow, UK), natural titanium (5 μm; 99.6% purity; Nilaco, Japan), and aluminum-27 (5 μm; >99% purity; Nilaco, Japan) foils. The yttrium foil was our main target to produce ^{89}Zr and ^{90}Nb. The titanium and aluminum foils were prepared for the monitor reactions and the energy degradation. The sizes and weights of the foils were measured to confirm the thickness of each foil. The deduced thicknesses were 24.2 μm for the yttrium foil, 5.1 μm for the titanium foil, and 5.5 μm for the aluminum foil. The three types of foils were cut to the size of 1 cm $\times$ 1 cm and were stacked in a target holder, which also served as a Faraday cup. The configuration of the stacked-foil target is listed in Table 1.

Table 1: Configuration of the stacked foils. The first foil was faced on the incident α beam.

Foil number	Foil element	Foil number	Foil element
1	Y	31	Ti
2	Al	32	Ti
3	Y	33	Y
4	Al	34	Ti
5	Y	35	Ti
6	Al	36	Y
7	Y	37	Ti
8	Al	38	Ti
9	Y	39	Y
10	Al	40	Ti
11	Y	41	Ti
12	Al	42	Y
13	Y	43	Ti
14	Al	44	Ti
15	Y	45	Y
16	Al	46	Ti
17	Y	47	Ti
18	Al	48	Y
19	Y	49	Ti
20	Al	50	Ti
21	Y	51	Y
22	Al	52	Ti
23	Y	53	Ti
24	Al	54	Y
25	Y	55	Ti
26	Al	56	Ti
27	Y	57	Y
28	Ti	58	Ti
29	Ti	59	Ti
30	Y		

2.2. Beam information

The stacked target was irradiated for 1 h with a 50.9 ± 0.1-MeV alpha beam, which was accelerated using the AVF cyclotron at RIKEN RI beam factory. The incident energy of the alpha beam was measured by the time-of-flight (TOF) measurement system[16] and its energy degradation in the target was calculated using the stopping powers of the foils. The stopping powers were obtained from the SRIM code[17]. The beam intensity was measured by the Faraday-cup-like target holder. The beam energy degradation and intensity were verified using the $^{27}\mathrm{Al}(\alpha, \mathrm{x})^{22}\mathrm{Na}$ and $^{\mathrm{nat}}\mathrm{Ti}(\alpha, \mathrm{x})^{51}\mathrm{Cr}$ monitor reactions in comparison with the IAEA's recommended cross sections. It was confirmed that cross sections of the monitor reactions were consistent with the recommended values by adjusting the beam intensity by -4% from the measured ones (see Fig. 1). The intensity (198 pnA) was assumed to be constant in the stacked target.

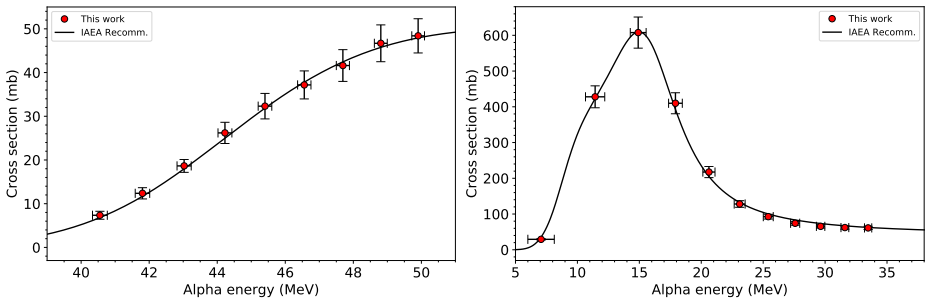

(a) $^{27}\mathrm{Al}(\alpha, \mathrm{x})^{22}\mathrm{Na}$ (b) $^{\mathrm{nat}}\mathrm{Ti}(\alpha, \mathrm{x})^{51}\mathrm{Cr}$

Figure 1: Measured cross sections for the $^{27}\mathrm{Al}(\alpha, \mathrm{x})^{22}\mathrm{Na}$ and $^{\mathrm{nat}}\mathrm{Ti}(\alpha, \mathrm{x})^{51}\mathrm{Cr}$ monitor reactions compared with the IAEA's recommended values.

2.3. Gamma-ray spectrometry

After the end of bombardment (EOB), the target was dismantled from the target holder for the off-line γ-ray spectrometry. High purity germanium (HPGe) detectors (ORTEC GMX-25190-P and GMX30P4-70) were used for the measurement. The detector efficiency was calibrated at each distance using the standard ^{152}Eu source and mixed source, which contains ^{57,60}Co, ^{85}Sr, ^{88}Y, ^{109}Cd, ^{133}Sn, ^{137}Cs, ^{139}Ce, ^{203}Hg, and ^{241}Am. The energy-efficiency curve was fitted using the following equation[18]:

$$\ln \varepsilon_\gamma = \sum_{i=0}^{5} p_i (\ln E_\gamma)^i \tag{1}$$

where p_i is the fitting coefficient, ε_γ is the photo-peak efficiency of the detector, and E_γ is the energy of the γ-ray emitted from the radionuclide. The analysis of the γ-line was performed using the software Gamma Studio (SEIKO EG&G).

The decay data for measured radionuclides, half-life, γ-line energy, and intensity were collected from NuDat2.7[19]. They are summarized in Table 2 with Q-value and threshold energy, which were obtained using the Q-value calculator (QCalc)[20].

Compensation of the recoil effect was taken into account by measuring the target foil and its subsequent foil together (see Table 1). The dead time was kept under 10% by adjusting the distances between the measured foil and the HPGe detector.

Table 2: Reaction and decay data of measured radionuclides. Note that only the reactions with the lowest threshold energy are listed.

Radionuclide	Decay mode	Half-life	E_γ (MeV)	I_γ (%)	Production routes	Q-value (MeV)	Threshold energy (MeV)
^{92m}Nb	β^++EC: 100%	10.15 d	934.44	99.15	^{89}Y(α, n)	-6.9	7.2
^{91m}Nb	IT: 96.6%	60.86 d	1204.67	2.0	^{89}Y(α, 2n)	-14.8	15.5
	β^++EC: 3.4%						
^{90g}Nb	β^++EC: 100%	14.6 h	141.178	66.8	^{89}Y(α, 3n)	-26.8	28.0
^{89m}Nb	β^++EC: 100%	66 m	588	95.57	^{89}Y(α, 4n)	-36.9	38.6
^{89g}Nb	β^++EC: 100%	2.03 h	1627.2	3.5	^{89}Y(α, 4n)	-36.9	38.6
^{89g}Zr	β^++EC: 100%	78.41 h	909.15	99.04	^{89}Y(α, tn)	-23.4	24.5
					Decay of ^{89m,g}Nb		
^{88g}Zr	EC: 100%	83.4 d	392.87	97.29	^{89}Y(α, t2n)	-32.7	34.2
^{90m}Y	IT: 100%	3.19 h	202.53	97.3	^{89}Y(α, ^{3}He)	-13.7	14.3
^{88g}Y	β^++EC: 100%	106.63 d	898.042	93.7	^{89}Y(α, αn)	-11.5	12.0
					Decay of ^{88g}Zr		
^{87m}Y	IT: 98.43%	13.37 h	380.79	78.05	^{89}Y(α, α2n)	-20.8	21.8
	β^-: 1.57%						
^{87g}Y	β^++EC: 100%	79.8 h	484.805	89.8	^{89}Y(α, α2n)	-20.8	21.8
					Decay of ^{87m}Y		
^{22}Na	β^+: 100%	2.6018 y	1274.537	99.940	^{27}Al(α, 2αn)	-22.5	25.9
^{51}Cr	β^++EC: 100%	27.7025 d	320.0824	9.910	^{47}Ti(α, γ)	8.94	0.0
					^{48}Ti(α, n)	-2.69	2.91
					^{49}Ti(α, 2n)	-10.8	11.7
					^{50}Ti(α, 3n)	-21.8	23.5

2.4. Cross-section derivation

To derive the cross sections using the measured γ-line counts, the following well known equation was used:

$$\sigma = \frac{\lambda C}{n_T \varphi \varepsilon_\gamma I_\gamma (1 - e^{-\lambda T_b}) e^{-\lambda T_c} (1 - e^{-\lambda T_m})} \tag{2}$$

where σ is the cross section, λ is the decay constant of each radionuclide, C is the γ-line counts, n_T is the atomic number areal density of the target, φ is the beam intensity, ε_γ is the detector efficiency, I is the intensity of the γ-line, and $T_b,\ T_c,\ T_m$ are the irradiation time, the cooling time, and the measurement time, respectively.

The total relative uncertainty of the cross section was evaluated by the following root square mean:

$$\Delta\sigma = \sqrt{(\Delta C)^2 + (\Delta n_T)^2 + (\Delta\varphi)^2 + (\Delta\varepsilon_\gamma)^2 + (\Delta I_\gamma)^2} \tag{3}$$

where $\Delta C,\ \Delta n_T,\ \Delta\varphi,\ \Delta\varepsilon_\gamma$, and ΔI_γ are the relative uncertainty of $C,\ n_T,\ \varphi,\ \varepsilon_\gamma$, and I_γ, respectively. Note that the uncertainties of the decay constant and times were ignored due to their negligible contribution.

3. Results and Discussion

Activation cross sections for 11 radionuclides ^{92m,91m,90,89m,89g}Nb, ^{89,88g}Zr, and ^{90m,88g,87m,87g}Y were deduced. The results are listed in Table 3 and shown in Fig. 2-12 with the earlier experimental [9, 10, 11, 12, 13] and TENDL-2017 data[15].

The total uncertainties of the derived cross sections were 7.2 to 24% including statistical uncertainties in γ-line counts (0.2-23%) and systematic uncertainties of the target thickness (1%), the alpha beam intensity (5%), the detector efficiency (5%), and the γ intensity (0.1-15%).

Table 3: Measured cross sections in the ^{89}Y(α, x) reaction.

	Cross section (mb)										
E (MeV)	^{92m}Nb	^{91m}Nb	^{90}Nb	^{89m}Nb	^{89g}Nb	^{89}Zr	^{88}Zr	^{90m}Y	^{88}Y	^{87m}Y	^{87g}Y
50.4 ± 0.6	1.24 ± 0.10		410 ± 30	19.6 ± 1.6	264 ± 29	533 ± 38	3.20 ± 0.35	9.02 ± 0.84	63.7 ± 4.7	116 ± 10	141 ± 10
49.4 ± 0.6	1.49 ± 0.12		532 ± 39	17.5 ± 1.5	227 ± 27	506 ± 36	2.44 ± 0.28	10.2 ± 0.9	71.0 ± 5.2	126 ± 11	156 ± 11
48.3 ± 0.6	1.58 ± 0.12		566 ± 41	13.7 ± 1.2	183 ± 24	376 ± 27	1.54 ± 0.19	8.44 ± 0.74	66.8 ± 4.9	109 ± 9	135 ± 10
47.1 ± 0.6	1.56 ± 0.12		618 ± 45	9.60 ± 0.80	107 ± 19	280 ± 20	1.08 ± 0.15	7.37 ± 0.68	63.4 ± 4.6	98.6 ± 8.6	121 ± 9
46.0 ± 0.6	1.97 ± 0.15		787 ± 57	7.28 ± 0.70	93 ± 19	239 ± 17	0.82 ± 0.14	8.09 ± 0.75	77.2 ± 5.6	98.9 ± 8.6	131 ± 9
44.8 ± 0.6	1.97 ± 0.15		796 ± 58	4.23 ± 0.52		141 ± 10		6.37 ± 0.60	72.4 ± 5.3	77.5 ± 7.2	105 ± 7
43.6 ± 0.6	2.32 ± 0.17		880 ± 63	1.61 ± 0.34		84.9 ± 6.1		5.20 ± 0.53	77.4 ± 5.6	71.4 ± 6.9	91.6 ± 6.6
42.4 ± 0.6	2.07 ± 0.16		777 ± 56			38.1 ± 2.7		3.73 ± 0.41	67.6 ± 4.9	49.9 ± 5.4	62.7 ± 4.5
41.2 ± 0.6	2.85 ± 0.21		939 ± 67			22.0 ± 1.6			84.6 ± 6.1	40.0 ± 4.7	57.1 ± 4.1
39.9 ± 0.6	2.70 ± 0.20		789 ± 57			8.33 ± 0.61			74.2 ± 5.4	24.8 ± 4.0	32.9 ± 2.4
38.6 ± 0.7	3.13 ± 0.22	16.2 ± 2.0	836 ± 60			4.36 ± 0.31			81.3 ± 5.8	17.7 ± 3.7	22.4 ± 1.6
37.3 ± 0.7	3.68 ± 0.26	22.7 ± 2.9	804 ± 58			2.68 ± 0.19			82.4 ± 5.9		11.5 ± 0.8
35.9 ± 0.7	3.18 ± 0.23	17.3 ± 3.2	536 ± 39			1.32 ± 0.10			59.0 ± 4.3		3.58 ± 0.26
34.5 ± 0.7	3.54 ± 0.26	28.0 ± 6.2	432 ± 32			0.767 ± 0.080			53.3 ± 3.9		1.22 ± 0.11
32.7 ± 0.7	4.20 ± 0.31	35.0 ± 6.2	270 ± 20			0.443 ± 0.068			44.4 ± 3.3		0.192 ± 0.046
30.8 ± 0.7	6.21 ± 0.45	54.9 ± 7.5	114 ± 9			0.240 ± 0.052			41.0 ± 3.0		
28.8 ± 0.8	8.15 ± 0.59	89.4 ± 9.9	6.4 ± 1.2						27.6 ± 2.1		
26.7 ± 0.8	10.0 ± 0.7	112 ± 11							14.4 ± 1.1		
24.5 ± 0.9	12.1 ± 0.9	110 ± 11							3.97 ± 0.41		
22.1 ± 0.9	22.3 ± 1.6	135 ± 22									
19.5 ± 1.0	62.0 ± 4.5	106 ± 26									
16.7 ± 1.2	233 ± 17										
13.5 ± 1.3	141 ± 10										
9.7 ± 1.5	7.35 ± 0.56										

3.1. $^{89}\mathrm{Y}(\alpha,\mathrm{n})^{92\mathrm{m}}\mathrm{Nb}$

The cross sections of $^{92\mathrm{m}}$Nb were derived using the γ-line at 934.44 keV ($T_{1/2}$ = 10.15 d, I_γ = 99.15%) after 10 days of the cooling time. The derived cross sections were compared with the earlier four experiments[9, 11, 12, 13] and TENDL-2017 data[15] and shown in Fig. 2. The tendency of the excitation function is similar to the data by M. Shahid *et al.*[11] and the TENDL-2017 data, but the location of the peak around 16 MeV is different from each other.

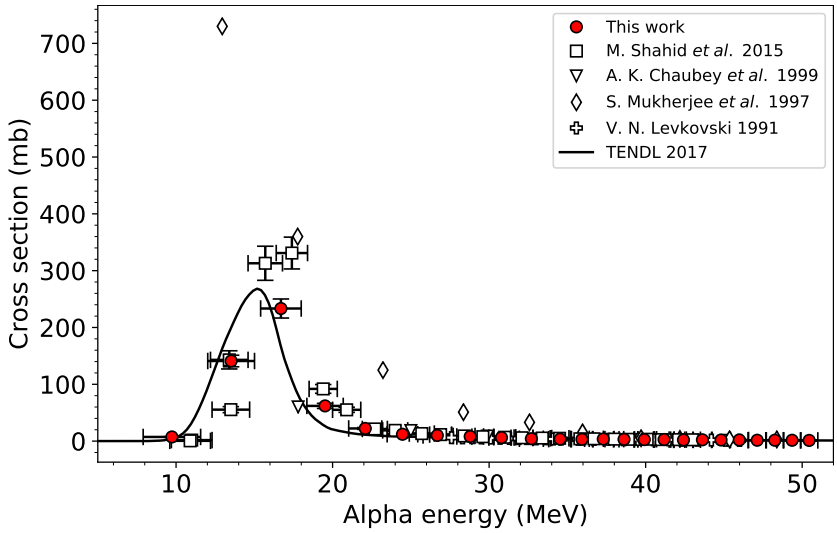

Figure 2: The cross sections of the $^{89}\mathrm{Y}(\alpha,\mathrm{n})^{92\mathrm{m}}\mathrm{Nb}$ reaction in comparison with the earlier experiments[9, 11, 12, 13] and TENDL-2017 data[15]

3.2. ^{89}Y$(\alpha, 2n)^{91m}$Nb

The excitation function of the ^{89}Y$(\alpha, 2n)^{91m}$Nb reaction was derived using the γ-line at 1204.67 keV ($T_{1/2}$ = 60.86 d, I_γ = 2.0%) after 10 days of the cooling time. There is one previous experimental dataset[11] for this reaction and it is compared with the derived excitation function in Fig. 3 in addition to the TENDL-2017 data[15]. The tendency of the two experimental datasets is consistent, but the cross section values in the low energy region were different. The TENDL-2017 data considerably overestimates the experimental data.

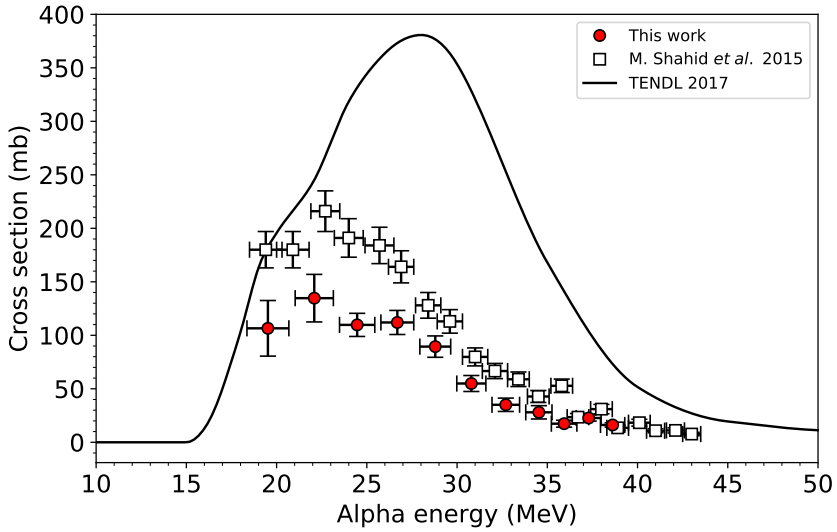

Figure 3: The cross sections of the ^{89}Y$(\alpha, 2n)^{91m}$Nb reaction in comparison with the earlier experiment[11] and TENDL-2017 data[15]

3.3. ^{89}Y$(\alpha, 3n)^{90}$Nb

The cross sections of ^{90}Nb were derived from the γ-line at 141.18 keV ($T_{1/2}$ = 14.6 h, I_γ = 92.7%) after 4 days of the cooling time. The metastable state ^{90m}Nb has a half-life of 18.81 s and decays to its ground state ^{90g}Nb by an IT process. Therefore the derived cross sections were cumulative. The dead time was 0.5-9%. The derived cumulative cross sections were compared with earlier five experimental datasets[9, 10, 11, 12, 13] and the TENDL 2017 library[15]. The peak position of the excitation function seems to be consistent with the previous three experiments[9, 11, 12], but our data are very scattered due to the large background located in the low energy region of the spectrum.

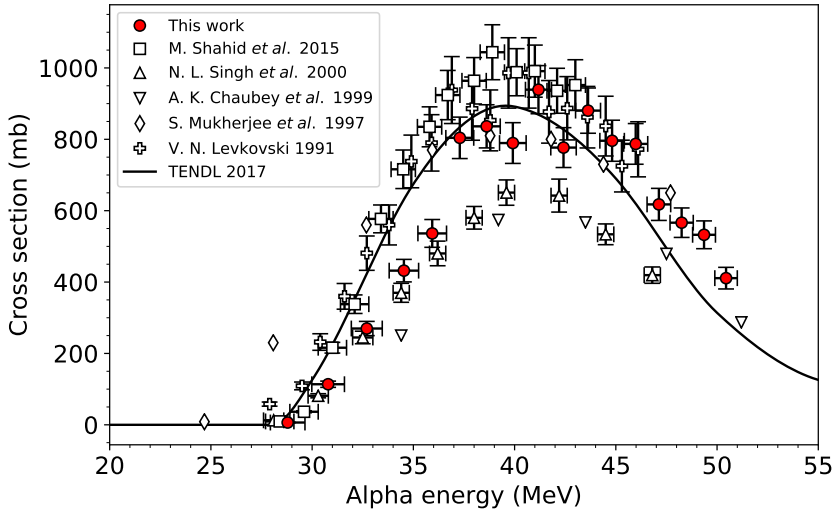

Figure 4: The cross sections of the ^{89}Y$(\alpha, 3n)^{90}$Nb reaction with the earlier experiments[9, 10, 11, 12, 13] and TENDL-2017 data[15]

3.4. ^{89}Y$(\alpha, 4n)^{89m}$Nb

The cross sections of ^{89m}Nb were derived from the γ-line at 588 keV ($T_{1/2}$ = 66 m, I_γ = 95.57%). The cooling time was 2-3 hours and the dead time was 5-7%. The cross sections of ^{89m}Nb are shown in Fig. 5 with one earlier experiment[11] and TENDL-2017 data[15]. As in the previous sections, data reported by Shahid *et al.*[11] are somewhat higher than our data. The theoretical data significantly overestimates the experimental data.

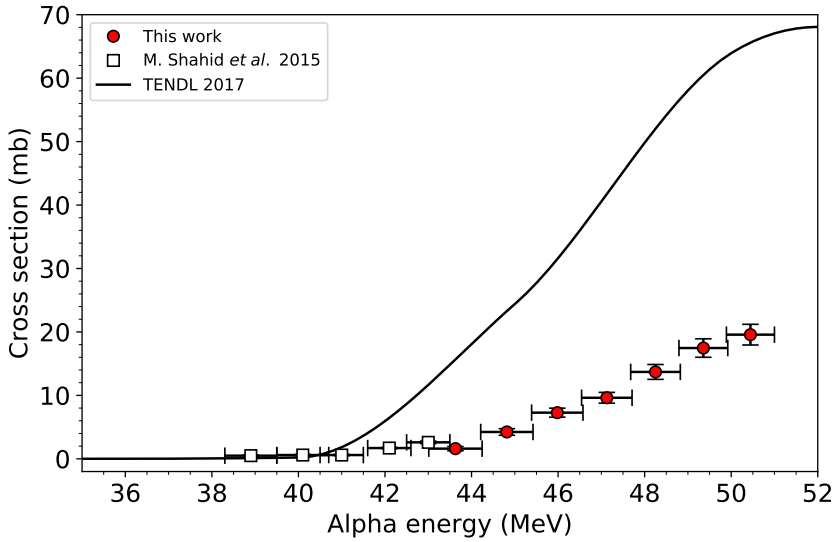

Figure 5: The cross sections of the ^{89}Y$(\alpha, 4n)^{89m}$Nb reaction in comparison with the earlier experiment[11] and TENDL-2017[15]

3.5. ^{89}Y$(\alpha, 4n)^{89g}$Nb

The excitation function of the ^{89}Y$(\alpha, 4n)^{89g}$Nb reaction was derived using the γ-line at 1627.2 keV ($T_{1/2}$ = 2.03 h, I_γ = 3.5%). The cooling time of 2-3 hours was taken and the dead time during this measurement was 5-6%. The result is shown with two earlier experimental datasets[11, 13] and TENDL-2017 data[15] in Fig. 6. The data above 46 MeV were newly obtained in this work. The experimental data of Chaubey *et al.*[13] are considerably lower than our data. The theoretical prediction overestimates the experimental data.

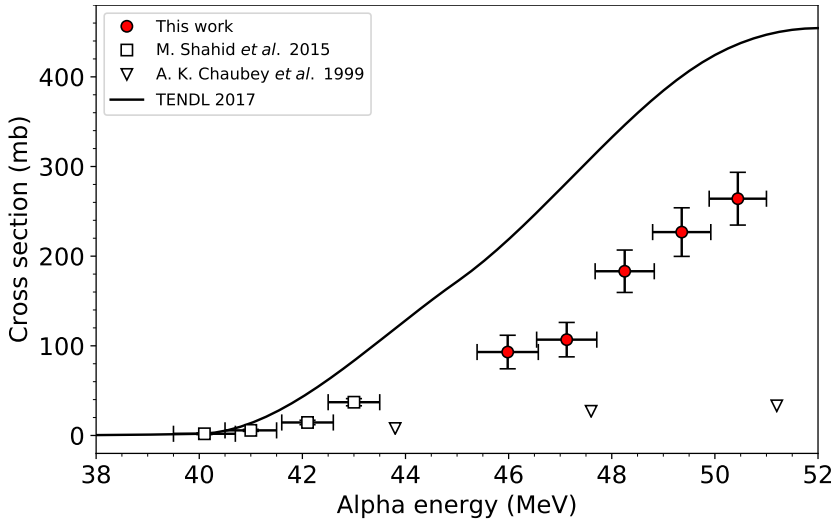

Figure 6: The cross sections of the ^{89}Y$(\alpha, 4n)^{89g}$Nb reaction in comparison with the earlier experiments[11, 13] and TENDL-2017 results

3.6. ^{89}Y$(\alpha, \mathrm{x})^{89\mathrm{g}}$Zr

The measurement was performed after the 10 days cooling time long enough for complete decay of $^{89\mathrm{g,m}}$Nb and ^{89}Zr to $^{89\mathrm{g}}$Zr. The cumulative cross sections of $^{89\mathrm{g}}$Zr were derived using the γ-line at 909.15 keV ($T_{1/2}$ = 78.41 h, I_γ = 99.04%). The dead time was 0.2-4% in this measurement.

There are three prior experimental datasets[9, 10, 11] for the cumulative cross sections of $^{89\mathrm{g}}$Zr. The comparison with the experimental results and the TENDL-2017 data[15] are shown in Fig. 7. Our measured data are consistent with the Levkovski's result[9], but the two other datasets are higher. The TENDL-2017 data overestimate in the higher energy region.

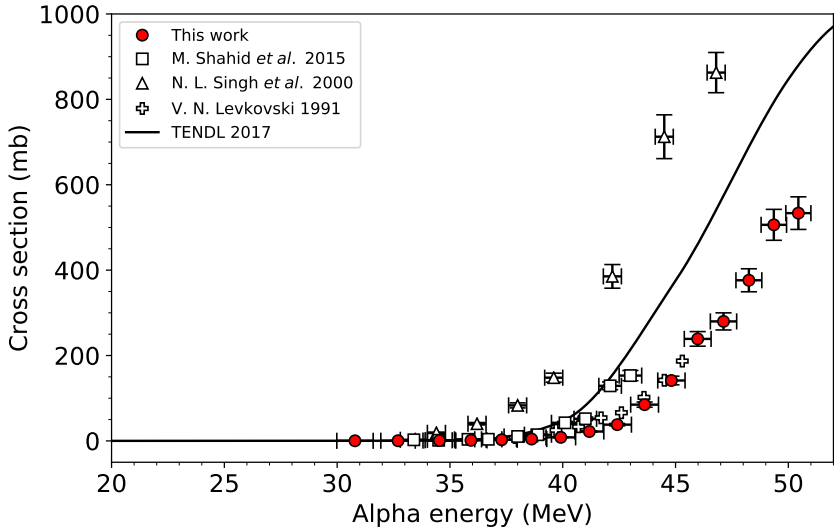

Figure 7: The cross sections of the ^{89}Y$(\alpha, \mathrm{x})^{89\mathrm{g}}$Zr reaction in comparison with the earlier experiments[9, 10, 11] and TENDL-2017 data[15]

3.7. ^{89}Y$(\alpha, \mathrm{x})^{88}$Zr

The excitation function of the ^{89}Y$(\alpha, \mathrm{x})^{88}$Zr reaction was derived using the γ-line of 392.87 keV ($T_{1/2}$ = 83.4d, I_γ = 97.29%). There are no contributions from ^{88}Nb since the threshold energy of the ^{89}Y$(\alpha, 4\mathrm{n})^{88}$Nb reaction is 51.7 MeV. The dead time was around 0.1% in this measurement after a cooling time of more than 1 year. The derived cross sections are shown in Fig. 8 with one earlier experiment dataset by M. Shahid *et al.*[11] and TENDL-2017 data[15]. New data were presented above 47 MeV in this work. The theoretical prediction soars in the high energy region compared with the present experimental values.

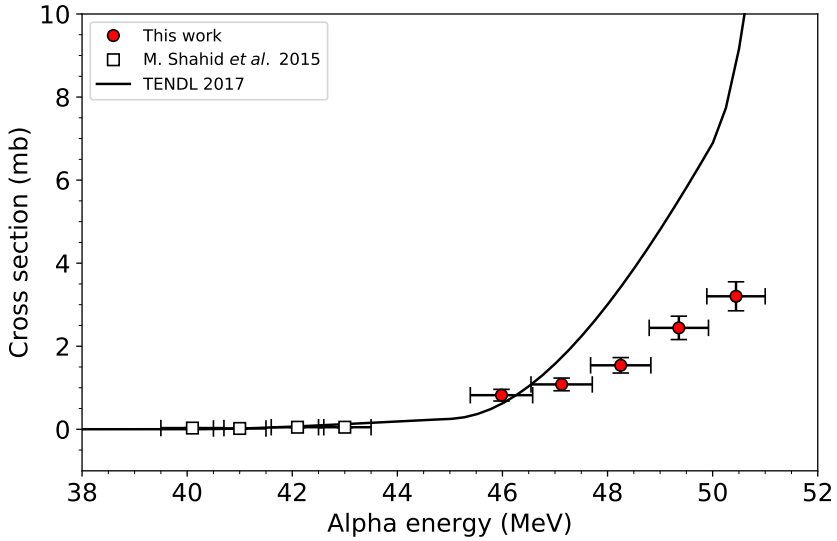

Figure 8: The cross sections of the ^{89}Y$(\alpha, \mathrm{x})^{88}$Zr reaction in comparison with the earlier experiment[11] and TENDL-2017 data[15]

3.8. $^{89}\mathrm{Y}(\alpha,\mathrm{x})^{90\mathrm{m}}\mathrm{Y}$

The cross sections of $^{90\mathrm{m}}$Y were derived after 2-3 hours of the cooling time using the γ-line at 202.53 keV ($T_{1/2} = 3.19$ h, $I_\gamma = 97.3\%$) with the dead time of 5-6%. The result is shown in Fig. 9 with one earlier experiment[11] and the TENDL-2017 data[15]. The measured cross sections present new data in the high energy region. Data of Shahid *et al.*[11] show somewhat a higher tendency than our experimental data. The TENDL-2017 data underestimate in the high energy region.

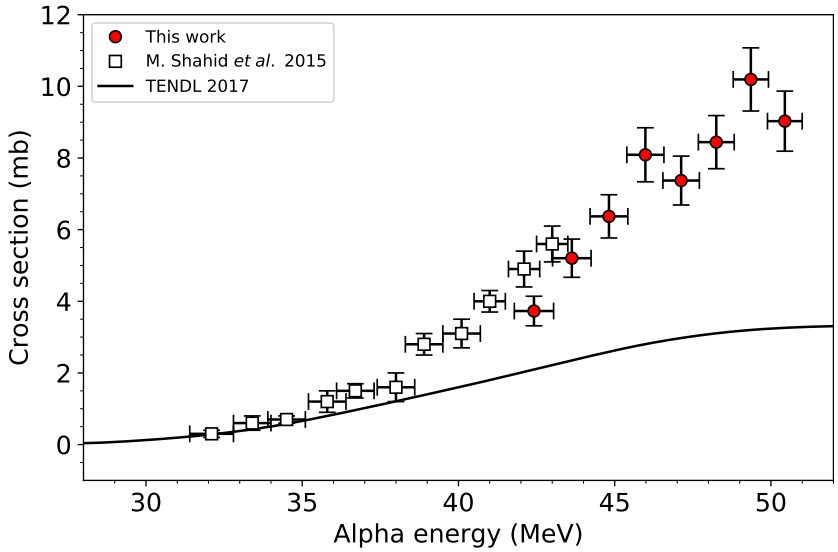

Figure 9: The cross sections of the $^{89}\mathrm{Y}(\alpha,\mathrm{x})^{90\mathrm{m}}\mathrm{Y}$ reaction in comparison with the earlier experiment[11] and the TENDL-2017 data[15]

3.9. ^{89}Y$(\alpha, \mathrm{x})^{88\mathrm{g}}$Y

The excitation function of the ^{89}Y$(\alpha, \mathrm{x})^{88\mathrm{g}}$Y reaction was derived from the γ-line at 898.042 keV ($T_{1/2}$ = 106.63 d, I_γ = 93.7%) after the 10-11 days cooling time. The dead time of this measurement was between 0.2 to 4%. The contribution from its parent radionuclide ^{88}Zr ($T_{1/2}$ = 83.4 d) can be estimated as 0.3% at most due to the relatively small cross sections of ^{88}Zr and was neglected. However, the cumulation via decay of the very short lived isometric states of ^{88}Y is included. The derived cross sections are shown with three earlier experiments and TENDL-2017 data in Fig. 10. The present data are consistent with the work by Levkovski[9] and the TENDL-2017 data above 37 MeV but are smaller than other data in the low energy region.

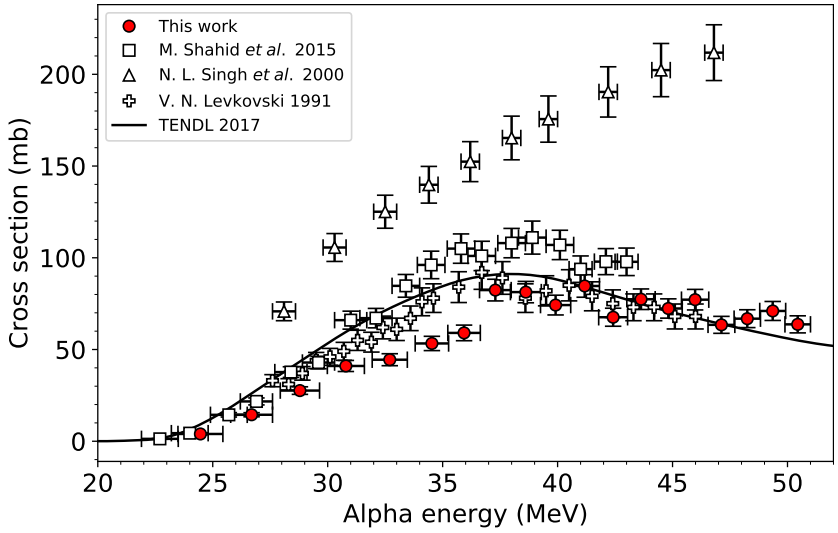

Figure 10: The cross sections of the ^{89}Y$(\alpha, \mathrm{x})^{88\mathrm{g}}$Y reaction in comparison with the earlier experiment[9, 10, 11] and TENDL-2017 data[15]

3.10. $^{89}\mathrm{Y}(\alpha,\mathrm{x})^{87\mathrm{m}}\mathrm{Y}$

The cross sections of the $^{89}\mathrm{Y}(\alpha,\mathrm{x})^{87\mathrm{m}}\mathrm{Y}$ reaction were derived after 4 days of cooling time using the γ-line at 380.79 keV ($T_{1/2} = 13.37$ h, $I_\gamma = 78.05\%$). The dead time was 4-9% in this measurement. The derived cross sections are shown in Fig. 11 with one earlier study[11]. The TENDL-2017 prediction is smaller than the present result in the higher energy region.

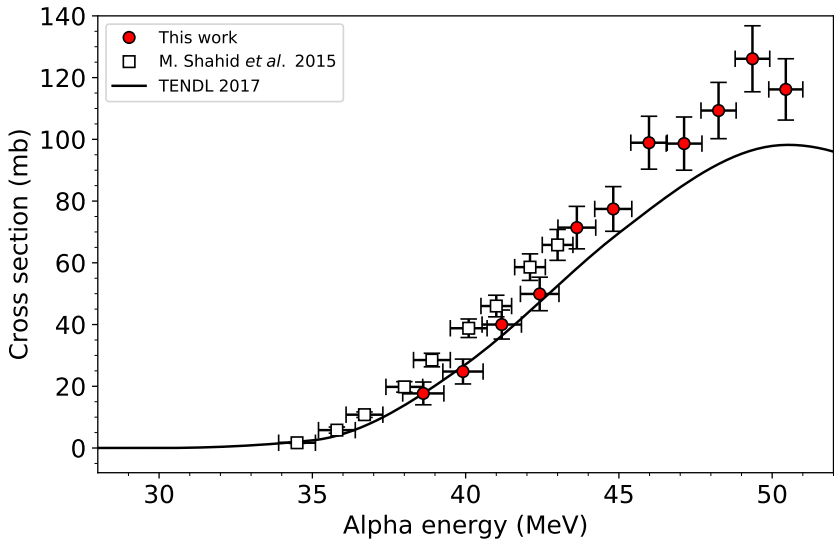

Figure 11: The excitation function of the $^{89}\mathrm{Y}(\alpha,\mathrm{x})^{87\mathrm{m}}\mathrm{Y}$ reaction in comparison with an earlier experiment[11] and TENDL-2017 data[15].

3.11. ^{89}Y$(\alpha, \mathrm{x})^{87\mathrm{g}}$Y

The ground state of ^{87}Y decays with a half-life of 79.8 hours and emits the γ-ray at 484.805 keV ($I_\gamma = 89.8\%$), which is used for the derivation of its excitation function. The cooling time was taken from 10 to 11 days to wait for the decay out of its isomeric state $^{87\mathrm{m}}$Y. Therefore, the cross sections shown in Fig. 12 are cumulative. Note that no contribution from the decay of ^{87}Zr was expected since the production of ^{87}Zr is not possible at the applied particle energy. The dead time in this measurement was 0.2-4%. There are three experimental datasets for the cumulative cross sections of $^{87\mathrm{g}}$Y, which are plotted together in Fig. 12. The tendencies are almost consistent with each other. However, the present data are larger than the others above 44 MeV.

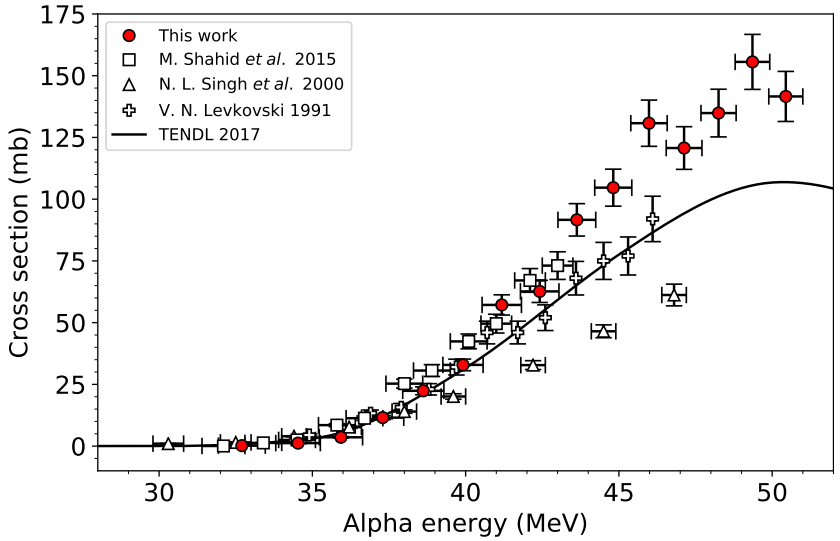

Figure 12: The excitation function of the ^{89}Y$(\alpha, \mathrm{x})^{87\mathrm{g}}$Y reaction in comparison with the earlier experiments[9, 10, 11] and TENDL-2017 data[15].

4. Conclusions

The excitation function measurement for α-induced reactions on yttrium-89 was performed up to 50 MeV. The main purpose of the study was to obtain the data for the ^{89}Zr and ^{90}Nb production, which are valuable for medical application. The cross sections of other co-produced radionuclides were also determined. Thus, the production cross sections of ^{92m,91m,90,89m,89g}Nb, ^{89,88g}Zr, ^{90m,88g,87m,87g}Y were obtained. The obtained cross sections were compared with the earlier experiments and TENDL-2017 library data. Our results were reasonably consistent with some of the previous studies. However, the peak position of the excitation function of ^{89}Zr is still not found, and the data for the ^{90}Nb is very scattered. As a future investigation, it would be worthwhile to solve these problems. To find the peak position for the ^{89}Y$(\alpha, \mathrm{x})^{89}$Zr reaction, the α-induced reaction using over 50 MeV is needed. On the other hand, in order to reduce the scattered data as seen in Fig. 4, using the lower intensity beam may be effective.

Declaration of Interest

Declarations of interest: none.

Acknowledgments

This work was carried out at RI Beam Factory operated by RIKEN Nishina Center and CNS, University of Tokyo, Japan. This work was supported by JSPS KAKENHI Grant Number 17K07004.

References

[1] A. M. Wu, P. D. Senter, Arming antibodies: Prospects and challenges for immunoconjugates, Nat. Biotechnol. 23 (9) (2005) 1137–1146. doi:10.1038/nbt1141.

[2] C. Bailly, P. François, A. Faivre-Chauvet, M. Bourgeois, F. Guérard, F. Haddad, J. Barbet, M. Chérel, F. Kraeber-Bodéré, T. Carlier, C. Bodet-Milin, Immuno-pet for clinical theranostic approaches, Int. J. Mol. Sci. 18 (1) (2017) 1–12. doi:10.3390/ijms18010057.

[3] G. A. van Dongen, G. W. Visser, M. N. Lub-de Hooge, E. G. de Vries, L. R. Perk, Immuno-PET: A Navigator in Monoclonal Antibody Development and Applications, Oncologist 12 (12) (2007) 1379–1389. doi:10.1634/theoncologist.12-12-1379.
URL http://theoncologist.alphamedpress.org/cgi/doi/10.1634/theoncologist.12-12-1379

[4] M. A. Deri, B. M. Zeglis, L. C. Francesconi, J. S. Lewis, PET imaging with 89Zr: From radiochemistry to the clinic, Nucl. Med. Biol. 40 (1) (2013) 3–14. doi:10.1016/j.nucmedbio.2012.08.004.
URL http://dx.doi.org/10.1016/j.nucmedbio.2012.08.004

[5] S. Heskamp, R. Raavé, O. Boerman, M. Rijpkema, V. Goncalves, F. Denat, 89Zr-Immuno-Positron Emission Tomography in Oncology: State-of-the-Art 89Zr Radiochemistry, Bioconjug. Chem. 28 (9) (2017) 2211–2223. doi:10.1021/acs.bioconjchem.7b00325.

[6] Y. W. Jauw, C. W. Menke-van der Houven van Oordt, O. S. Hoekstra, H. N. Hendrikse, D. J. Vugts, J. M. Zijlstra, M. C. Huisman, G. A. van Dongen, Immuno-positron emission tomography with zirconium-89-labeled monoclonal antibodies in oncology: What can we learn from initial clinical trials?, Front. Pharmacol. 7 (MAY) (2016) 1–15. doi:10.3389/fphar.2016.00131.

[7] V. Radchenko, D. V. Filosofov, O. K. Bochko, N. A. Lebedev, A. V. Rakhimov, H. Hauser, M. Eisenhut, N. V. Aksenov, G. A. Bozhikov, B. Ponsard, F. Roesch, Separation of 90Nb from zirconium target for application in immuno-pet, Radiochim. Acta 102 (5) (2014) 433–442. doi:10.1515/ract-2013-2156.

[8] V. Radchenko, S. Busse, F. Roesch, Desferrioxamine as an appropriate chelator for 90Nb: Comparison of its complexation properties for M-Df-Octreotide (M=Nb, Fe, Ga, Zr), Nucl. Med. Biol. 41 (9) (2014) 721–727. doi:10.1016/j.nucmedbio.2014.06.006.
URL http://dx.doi.org/10.1016/j.nucmedbio.2014.06.006

[9] V. N. Levkovski, Cross-section of medium mass nuclide activation (A=40-100) by medium energy protons and alpha particles, Inter-Vesi, Moscow, USSR, 1991.

[10] N. L. Singh, M. S. Gadkari, S. N. Chintalapudi, Measurement and Analysis of Alpha Particle Induced Reactions on Yttrium, Phys. Scr. 61 (5) (2000) 550–554. doi:10.1238/Physica.Regular.061a00550.
URL http://stacks.iop.org/1402-4896/61/i=5/a=008?key=crossref.a879258a5ada8d627358f8226d04f6a7

[11] M. Shahid, K. Kim, G. Kim, M. Zaman, M. Nadeem, Measurement of excitation functions in alpha induced reactions on nat Cu, Nucl. Instruments Methods Phys. Res. Sect. B Beam Interact. with Mater. Atoms 358 (2015) 160–167. doi:10.1016/j.nimb.2015.06.026.
URL http://dx.doi.org/10.1016/j.nimb.2014.09.028

[12] S. Mukherjee, B. B. Kumar, M. H. Rashid, S. N. Chintalapudi, α -particle induced reactions on yttrium and terbium, Phys. Rev. C 55 (5) (1997) 2556–2562. doi:10.1103/PhysRevC.55.2556.
URL https://link.aps.org/doi/10.1103/PhysRevC.55.2556

[13] A. K. Chaubey, I. A. Rizvi, Non-equilibrium effects in alpha induced reactions in some natural elements, Indian J. Pure Appl. Phys. 37 (11) (1999) 791–793.

[14] N. Otuka, E. Dupont, V. Semkova, B. Pritychenko, A. Blokhin, M. Aikawa, S. Babykina, M. Bossant, G. Chen, S. Dunaeva, R. Forrest, T. Fukahori, N. Furutachi, S. Ganesan, Z. Ge, O. Gritzay, M. Herman,

S. Hlavač, K. Katō, B. Lalremruata, Y. Lee, A. Makinaga, K. Matsumoto, M. Mikhaylyukova, G. Pikulina, V. Pronyaev, A. Saxena, O. Schwerer, S. Simakov, N. Soppera, R. Suzuki, S. Takács, X. Tao, S. Taova, F. Tárkányi, V. Varlamov, J. Wang, S. Yang, V. Zerkin, Y. Zhuang, Towards a More Complete and Accurate Experimental Nuclear Reaction Data Library (EXFOR): International Collaboration Between Nuclear Reaction Data Centres (NRDC), Nucl. Data Sheets 120 (2014) 272–276. doi:10.1016/J.NDS.2014.07.065.
URL https://www.sciencedirect.com/science/article/abs/pii/S0090375214005171?via{%}3Dihub

[15] A. Koning, D. Rochman, Modern Nuclear Data Evaluation with the TALYS Code System, Nucl. Data Sheets 113 (12) (2012) 2841–2934. doi:10.1016/J.NDS.2012.11.002.
URL https://www.sciencedirect.com/science/article/abs/pii/S0090375212000889?via{%}3Dihub

[16] T. Watanabe, M. Fujimaki, N. Fukunishi, H. Imao, O. Kamigaito, M. Kase, M. Komiyama, N. Sakamoto, K. Suda, M. Wakasugi, K. Yamada, Beam energy and longitudinal beam profile measurement system at the RIBF, Proc. 5th Int. Part. Accel. Conf. (IPAC 2014) (2014) 3566–3568doi:10.18429/JACoW-IPAC2014-THPME136.

[17] J. F. Ziegler, M. Ziegler, J. Biersack, SRIM – The stopping and range of ions in matter (2010), Nucl. Instruments Methods Phys. Res. Sect. B Beam Interact. with Mater. Atoms 268 (11-12) (2010) 1818–1823. doi:10.1016/J.NIMB.2010.02.091.
URL https://www.sciencedirect.com/science/article/pii/S0168583X10001862?via{%}3Dihub

[18] A. R. Usman, M. U. Khandaker, H. Haba, N. Otuka, M. Murakami, Y. Komori, Production cross-sections of radionuclides from α-induced reactions on natural copper up to 50 MeV, Appl. Radiat. Isot. 114 (2016)

104–113. doi:10.1016/J.APRADISO.2016.04.027.
URL https://www.sciencedirect.com/science/article/pii/S0969804316301580?via{%}3Dihub

[19] National Nuclear Data Center, Nudat 2.7 [cited 2019-06-23].
URL https://www.nndc.bnl.gov/nudat2/

[20] National Nuclear Data Center, Q-Value Calculator (QCalc) [cited 2019-06-22].
URL https://www.nndc.bnl.gov/qcalc/